Advanced Steel Construction – Vol. 22 No. 2 (2026) 208–221
DOI:10.18057/IJASC.2026.22.2.7

EXPERIMENTAL STUDY ON SEISMIC BEHAVIOR OF DOUBLE-SKIN COMPOSITE WALL WITH REBAR TRUSSES

Li-Ping Zhang [1, 4], Yan-Sheng Huang [1], Chun Yang [1, *], Chi-Yu Luo [2], Xing-Long Luo [3], Bing-Qiang Sui [3] and Jian Cai [1]

[1] *South China University of Technology, Guangzhou, 510641, China*
[2] *Guang Dong Architectural Design and Research Institute Corporation Limted, Guangzhou, 510010, China*
[3] *MCC Shanghai Steel Structure Technology Corporation Limted, Shanghai 201908, China*
[4] *CCCC-FHDI Engineering Corporation Limted, Guangzhou 510000，China*
** (Corresponding author: E-mail: 13392631280@189.cn)*

ABSTRACT

This paper introduces a novel double-skin composite wall (DSCW) system reinforced with horizontal rebar trusses. The seismic performance of five double-skin composite wall specimens with rebar trusses and one specimen without rebar trusses was investigated under low cyclic lateral loading. The test results demonstrate that all specimens reached a flexure-dominated ultimate state, accompanied by local buckling of the faceplates in the shear wall and the boundary columns of the concrete-filled steel tube (CFST). The five specimens reinforced with rebar trusses exhibited excellent ductile behavior, with ductility coefficients ranging from 1.86 to 2.78. Comparative analysis among the specimens revealed that the inclusion of rebar trusses effectively stabilized the faceplates and improved the overall performance of the composite walls. Closer spacing of the rebar trusses, such as 100 mm, proved to be more effective. Specimens with vertical and horizontal rebar trusses demonstrated similar peak load capacities; however, the specimen with vertical rebar trusses achieved a 6.0% higher ductility coefficient, indicating improved deformation capacity. Furthermore, the use of a discontinuous inner steel plate in the CFST boundary column was found to reduce both lateral load-carrying capacity and ductility, rendering it an unsuitable design choice for this system.

ARTICLE HISTORY

Received: 22 February 2025
Revised: 16 July 2025
Accepted: 18 July 2025

KEYWORDS

Double-skin steel-concrete composite wall;
Rebar trusses;
Quasi-static test;
Seismic performance

1. Introduction

The shear wall is a critical load-bearing and lateral force-resisting component in high-rise buildings. Existing prefabricated shear walls primarily include precast reinforced concrete walls, precast double-superimposed walls, pure steel plate walls, and double-skin steel-concrete composite walls. Precast reinforced concrete shear walls are heavy and challenging to install [1]. Precast double-superimposed walls have certain drawbacks, such as complex splicing construction, high installation precision requirements, and low reliability [2–5]. Pure steel plate walls, while effective for lateral resistance, have limited vertical load-carrying capacity [6]. As a novel type of composite component, the double-skin steel-concrete composite wall (DSCW) consists of concrete filled between two steel faceplates, which are connected by shear connectors. The steel plates and concrete work together compatibly throughout the entire loading process, significantly enhancing the wall's compressive, tensile, and shear capacities, as well as its energy dissipation performance.

In the 1980s, PF Adams, Hassinen, and Stephen [7–9] initiated research on DSCWs. Their studies primarily focused on the performance and failure mechanisms of DSCWs under the impact of ice and sea waves, demonstrating that DSCWs provide high strength and ductility when subjected to out-of-plane loads. Wright et al. [10–12] investigated the axial compression and shear performance of DSCWs with profiled steel sheeting and developed design formulas for shear strength and stiffness. Link [13] employed a nonlinear finite element method to study the ultimate bearing capacity and post-peak behavior of DSCWs under transverse and longitudinal loads. Emori [14] conducted experimental research on concrete-filled steel box walls under compressive and shear loading. The results revealed that the wall elements exhibited both high strength and excellent ductility. Nie et al. [15–17] designed a series of DSCW test specimens equipped with studs and load-bearing steel bars, with axial compression ratios ranging from 0.15 to 0.4. The test results showed that the average ultimate displacement angle of the walls was 1.7%, and the average ductility coefficient was 3.2. In further research, Nie [18] designed another set of DSCW test specimens with short stiffeners and studs, with a higher axial compression ratio of 0.5. The results indicated that the average ultimate lateral displacement angle of these walls was 1.6%.

To further improve buckling capacity of the DSCWs, experimental researches on DSCW strengthened with batten plate [19-20], tie rod [21-24], steel tube bundles [25-26], corrugated plates[27] and hybrid connectors [28] were conducted, test results concluded that the specimens had good ductility and energy dissipation capacity, and the hysteretic curves were full and stable.

While Shi et al. [29] adopted vertical rebar trusses to stabilize the steel faceplate of DSCW, experimental results found that reducing the welding spot spacing-to-thickness ratio and opening slits on the steel plate could increase the buckling capacity of the DSCW. Han et al. [30] also investigated the seismic behavior of DSCW stiffened with vertical steel truss, and found that aspect ratio had the greatest impact on the failure mode and seismic performance of the specimen, while the axial compression ratio had little impact on the strength. The ductility and energy consumption of specimens with small axial compression ratios are good, however. The larger the spacing of the steel truss, the weaker the out of plane constraint on the steel plate, and the earlier the appearance of the specimen’s buckling and failure.

Further parametic studies were carried out to investigate key parameters that affected the seismic performances of DSCW. Wei et al. [31] established the finite element model of DSCW and presented the effects of key parameters including the space of stud connectors, the thickness of both the steel plate and concrete core, the concrete strength, and the span-depth ratio of walls on the shear resistance of the walls. Results indicated that the thickness of both the steel plate and the concrete core, and the strength of concrete are the most critical factors affecting the shear resistance of the walls, and the spacing of stud connectors affects the failure mode of the walls. The influence of various parameters on the hysteretic behavior of the DSCW was studied by Luo et al. [32] through numerical analysis. Numerical evaluation reveals a substantive impact exerted by all three parameters upon the mechanical attributes of the wall. Of particular note, the axial compression ratio emerges as the predominant determinant influencing the wall's loading capacity, framed within this context. Furthermore, it becomes evident that the aspect ratio, characterized by its considerable elongation relative to width, coupled with the ratio of width-to-thickness, manifests as pivotal determinants dictating the initial stiffness attributable to the wall structure.

The studies mentioned above have significantly contributed to the advancement of the mechanical behavior and design theory of the DSCW structure. However, the structural forms of the wall studied are complex, and the construction process needs to be improved. The welding workload of steel plate wall in the form of batten plate is large, the welding deformation of thin steel plate is easy to form and difficult to rectify, the batten plate is limited by the width-thickness ratio of steel plate and the welding operation, the vertical joint should be added for long steel plate wall, which further increase the welding workload and the difficulty of correction. The requirement for reserve holes on the steel plate of the wall in the form of a restraining rod weakens the steel plate section. Additionally, additional stiffness strengthening measures are required to meet the deformation and site alignment requirements during the transportation and hoisting of high flexible steel plate walls, which is challenging to do during the actual construction of high-rise buildings. While the DSCW reinforced with vertical rebar trusses avoids some defects above, it provides weak transverse stiffness during construction.

Inspired by various designs of DSCW, this study proposes a novel DSCW system reinforced with horizontal rebar trusses. The proposed DSCW consists of concrete-filled square steel tubes (CFSTs) and a concrete-filled steel plate shear wall body, reinforced with horizontal rebar trusses, as illustrated in Fig. 1. Previous research [33] has shown that CFSTs significantly enhance the in-plane flexural capacity and out-of-plane flexural rigidity of walls, enabling them to meet maximum compressive demands more effectively.

The shear wall web is composed of concrete, rebar trusses, and two steel faceplates welded to the CFST. Each rebar truss comprises one longitudinal bar (acting as the chord member) and diagonal bars. The diagonal bars are spot-welded to the steel faceplates. Under compression, the synergy between the diagonal bars, chord bar, and steel faceplates effectively constrains the infilled concrete, while also stabilizing the steel faceplates during transportation and hoisting. Before the infilled concrete sets, the horizontal rebar trusses enhance the wall's out-of-plane flexural capacity and rigidity. In addition to improving rigidity, the horizontal rebar trusses, in conjunction with the steel faceplates, serve as the primary shear reinforcement to resist in-plane shear forces. They also act as formwork, enabling convenient and rapid construction without the need for additional construction aids. Furthermore, the rebar trusses are arranged separately, meaning they are independently welded to the steel faceplates. This eliminates the need for welding in enclosed spaces during the production of the steel plate wall, facilitating factory-based manufacturing of the composite wall.

Experimental research on the mechanical properties of six DSCW specimens with fixed axial compression ratio and span ratio under low cycle reciprocating loads was conducted in this paper. The key parameters considered include the spacing and direction of the steel truss, as well as the continuity of the steel plates in the shear wall adjacent to the CFST. The influence of each parameter on the seismic performance of the new composite wall, such as bearing capacity, ductility, stiffness and strength degradation, and energy dissipation capacity, was studied.

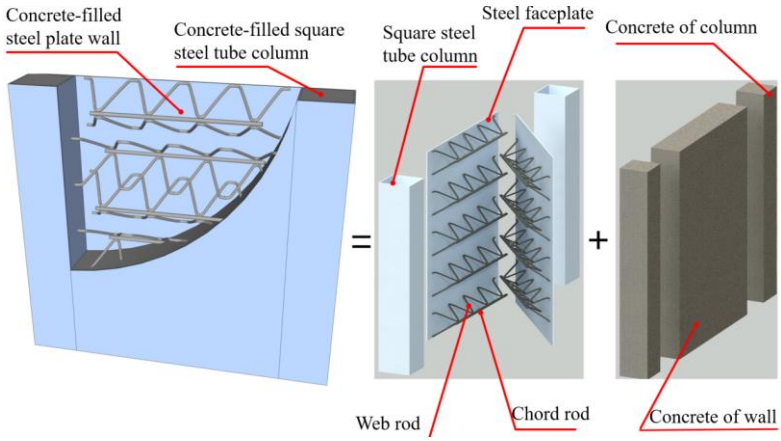

Fig. 1 Proposed DSCW with horizontal rebar trusses

2. Experimental program

2.1. Test specimens

Six specimens were designed and constructed for this study, including five DSCWs with rebar trusses and one DSCW without rebar trusses for comparison. The DSCWs with rebar trusses consisted of concrete-filled square steel tubes (CFSTs) and a concrete-filled steel plate wall body reinforced with separately arranged rebar trusses. To ensure direct comparison, all specimens had identical dimensions, with a net height of 1300 mm, a width of 650 mm, and a thickness of 100 mm. The specimens were embedded into rigid foundation beams and caps at both ends. The square steel tubes had a wall thickness of 4 mm, while the steel faceplates of the shear wall were 3 mm thick. The diameters of the web and chord bars in the rebar trusses were 6 mm and 8 mm, respectively. Notably, no additional shear connectors were incorporated into the DSCW specimens.

Two key parameters were investigated in this study. First, the spacing of the rebar trusses was identified as a critical factor influencing the bearing capacity and failure mode, particularly the local buckling behavior. Second, the orientation of the rebar trusses, whether embedded horizontally or longitudinally in the shear wall, was examined for its impact on the flexural and shear capacity as well as the rigidity of the wall.

Additionally, a trial parameter was introduced to explore construction feasibility. Since the CFST serves as the edge component, welding the inner steel plate of the square steel tube becomes challenging when connecting walls between floors. To address this issue, one specimen was designed with a discontinuous inner steel plate in the CFST, achieved by cutting the inner steel plate below the top of the beam. This modification was a preliminary attempt to determine whether this structural form could be viable for practical applications.

To isolate the effects of the aforementioned parameters on the mechanical behavior of the specimens, other key factors, such as the axial compression ratio and the height-to-width ratio, were held constant. In this study, the height-to-width ratio of all specimens was set to 2.0 to ensure the preferred flexural limit state [34], while the axial compression ratio was maintained at 0.40, consistent with values commonly used in engineering applications. Future experimental studies will further explore the effects of axial compression ratio and height-to-width ratio on the mechanical behavior of the newly designed DSCWs.

The structural details of all specimens are shown in Table 1 and Fig. 2. The axial compression ratio of the specimen was calculated using Eq. (1) as below:

$$n_t = N/(f_{ck}A_c + f_yA_a) \quad (1)$$

where n_t is the test axial compression ratio applied to the specimen, N is the test value of axial compression, f_{ck} is the material compressive strength of concrete infill, f_y is the yield strength of steel faceplate and steel tubes, A_c is the area of concrete wall, A_a is the sum of cross-sectional areas of steel tube and steel plate.

Table 1
Demensions and configurations of six test specimens

Specimen	$H \times h_w \times b_w$/mm	n_t	λ	Rebar trusses		Continuity of the CFST inner steel plate
				Spacing/mm	Direction	
SCW-1	1300x650x100	0.40	2.0	(without rebar trusses)		Continuous
SCW-2	1300x650x100	0.40	2.0	100	Horizontal	Continuous
SCW-3	1300x650x100	0.40	2.0	140	Horizontal	Continuous
SCW-4	1300x650x100	0.40	2.0	200	Horizontal	Continuous
SCW-5	1300x650x100	0.40	2.0	100	Vertically	Continuous
SCW-6	1300x650x100	0.40	2.0	100	Horizontal	Discontinuity

Note: H is the height from the loading point to the bottom of the wall, h_W and b_W are the height and thickness of the cross section respectively, n_t is the test axial compression ratio, and λ is the aspect ratio.

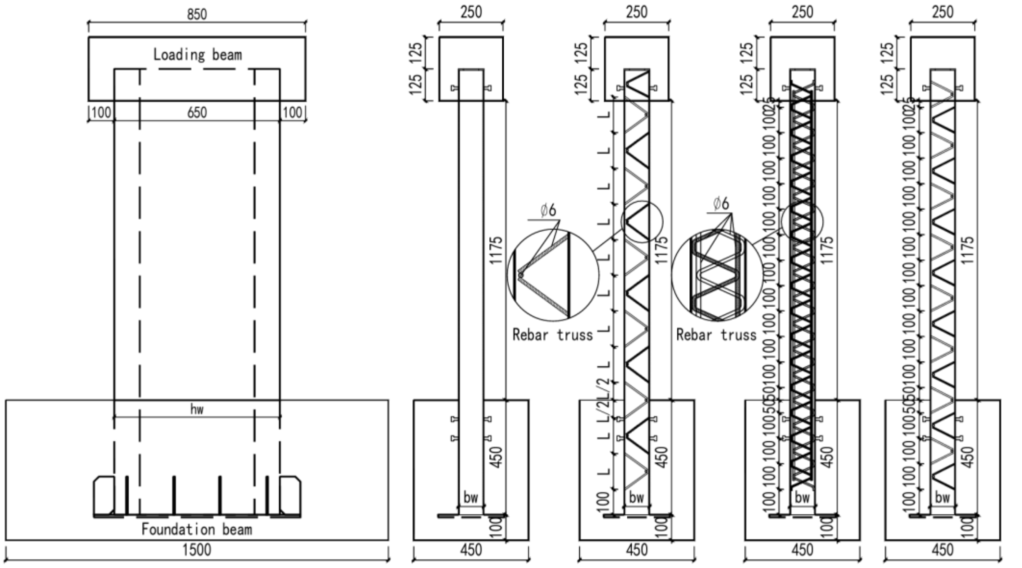

(a) Front elevation (b) SCW1 (c) SCW2-4 (d) SCW5 (e) SCW6

Fig. 2 Layout of the test specimens (mm)

The material properties of the steel plates and rebars were determined through monotonic tensile tests conducted on standard coupons. The measured values are summarized in Table 2. All specimens were cast using the same batch of concrete, and the average compressive strength of the concrete, measured using standard cube specimens (150 mm × 150 mm × 150 mm), was 55.35 MPa.

Table 2
Material properties of steel plate and steel bar

Material type	f_y/MPa	f_u/MPa	E_s/GPa
Steel plate	366.50	468.00	196.91
Steel bar	404.11	470.74	242.09

2.2. Test setup and loading protocol

The test was carried out in the structural laboratory of State Key Laboratory of Subtropical Building Science, South China University of Technology. All specimens were tested as walls with the fixed-end condition using the test setup shown in Fig.3. As illustrated, a concrete loading beam with a section of 250 x 250 mm was set on the top of the specimen. The bottom of each specimen was fixed to a foundation beam. The rigid foundation beam was poured at the bottom of the specimen to ensure that the bottom of the wall met the boundary conditions of fixed constraints. Both ends of the foundation beam were fixed on a rigid base plate with ground anchor bolts, and horizontal jacks were set at both ends of the foundation beam to prevent horizontal sliding of the foundation beam during loading. The horizontal reciprocating load was applied by a 1000 kN MTS hydraulic servo actuator connected to a rigid loading beam, and they were loaded at the center of the loading beam. The actuator and the loading beam were fixed by the loading head, and the rear end of the actuator was fixed to the reaction wall.

The vertical load was applied by a vertical inverted hydraulic jack, a sliding support was installed between the jack and the reaction frame to ensure that the loading point of the vertical load was always along the centerline of the wall, and to synchronize with the deformation of the specimen during loading process. A steel beam was set between the vertical jack and specimen to evenly apply vertical load on the wall. During the test, lateral support was set outside the plane of the specimen to avoid instability outside the plane. The device was a rigid beam with horizontal sliding bearing, which was fixed on the reaction base plate by rigid support to achieve in-plane working conditions of the specimens.

During the experiment, the vertical load was constant, and the MTS hydraulic servo actuator was used to apply the horizontal cycling load. The drift angle of the wall was considered as the control value during the entire loading process. At the beginning of loading, the displacement scheme was cycled only once until the steel plate at the bottom of CFST yielded, then the lateral displacement was imposed on the specimens with three cycles of loading at each step. The loading history is shown in Fig. 4. The test terminated when the specimen could not maintain the applied axial load or the horizontal peak load degraded 15% or more.

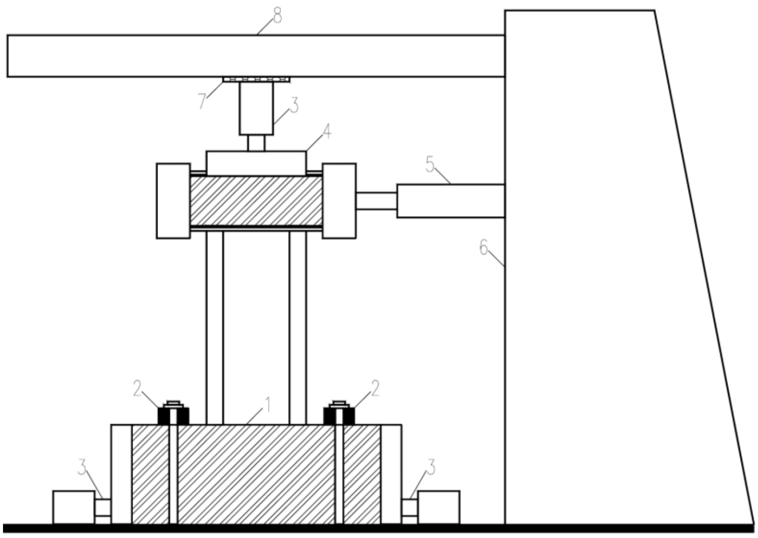

1. Foundation beam; 2. Beam; 3. Jack; 4. Distribution beam; 5. Actuator; 6. Reaction wall; 7. Sliding support; 8. Reaction frame
(a) Sketch of test setup

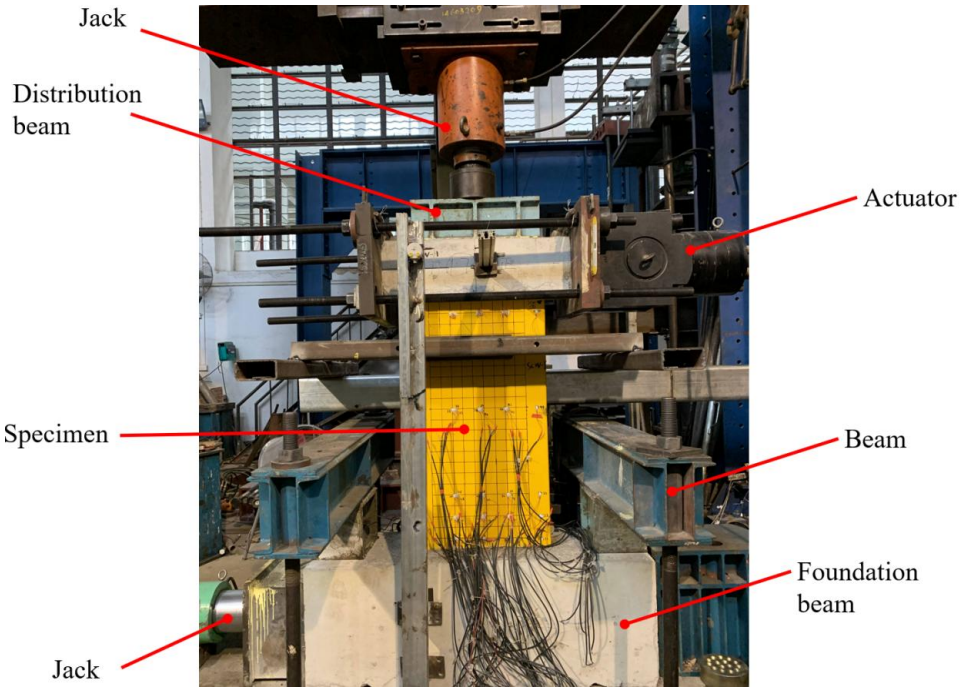

(b) Test setup in SCUT's lab

Fig. 3 Test setup

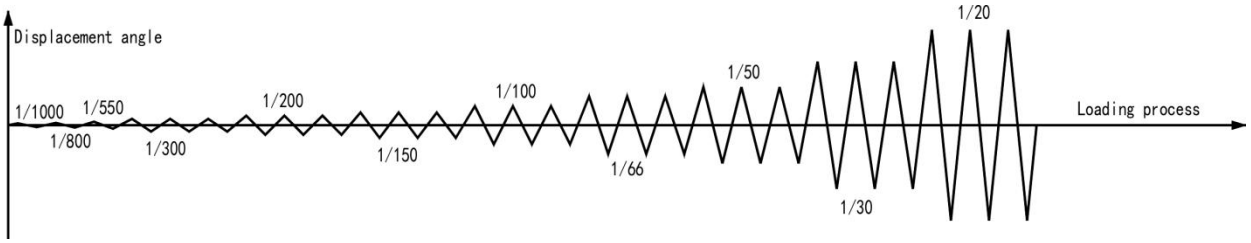

Fig. 4 Loading protocol

The experimental test setup used in this study is illustrated in Fig. 3, consisting of eight key components: the foundation beam, steel beam, test specimen, jack, distribution beam, actuator, reaction wall, sliding support, and reaction frame. The foundation beam and reaction frame were designed to provide a rigid base and structural support for the test specimens, while the jack and actuator applied lateral loading to simulate in-plane forces. The distribution beam ensured uniform load transfer to the specimen, and a sliding support was incorporated to allow for controlled movement during testing. The entire setup was constructed in SCUT's laboratory, as shown in Fig. 3(b), to facilitate accurate measurement of the mechanical behavior of the shear wall specimens under cyclic loading conditions. The corresponding loading protocol is depicted in Fig. 4.

2.3. Measurement method

Five displacement meters and fifty-three strain gauges were employed to record the displacement and strain responses of each specimen. The horizontal load was automatically measured using the MTS servo-hydraulic actuator's built-in measuring system. Displacement meters No. 1 to 3 were positioned to measure the in-plane lateral displacement at three key locations along the wall height: the center of the cap, the midpoint, and 150 mm above the footing. Additionally, two wire-type displacement meters were arranged diagonally on the wall to capture its shear deformation.

A total of fifty-three strain gauges were strategically placed along the CFST and the steel faceplates to monitor strain responses at critical locations. The detailed arrangement of the instrumentation is illustrated in Figs. 5 and 6.

3. Test results and discussion

3.1. Damage progression and failure modes

Upon the application of an axial compression load of 1700 kN, no visible overall or local displacement was observed in the specimens. As lateral loading was progressively applied to a peak drift angle of 1/550, only the outer steel plate of SCW-1's CFST reached its yield point. When the peak drift angle increased to the first cycle of 1/300, a slight "rustling" sound was detected, indicating local bonding failure at the interface between the steel faceplate and the infill concrete of SCW-1. At this stage, the outer steel plates of the CFST in all newly developed DSCW specimens (SCW-2 to SCW-6) began to yield. After three cycles of loading, all specimens produced a similar "rustling" sound.

The first instance of local buckling was observed in specimen SCW-1 during the first cycle at a peak drift angle of 1/200, where a bulge of approximately 5–10 mm appeared on the front and back steel faceplates, located 100 mm above the foundation beam. In specimen SCW-3, which featured horizontal rebar trusses with a spacing of 140 mm, local buckling occurred at the end of the 1/200 drift angle loading, resulting in a 3–5 mm bulge at a height of 250 mm. Similarly, in specimen SCW-4, local buckling appeared as a 2–3 mm bulge on the left side of the front steel faceplate at a height of 200 mm during loading to a drift angle of 1/150. After three loading cycles, the local buckling in SCW-3 expanded slightly, and the right side of the front plate in SCW-4's wall body developed minor local buckling at the same height of 200 mm.

No local buckling or visible damage was observed in the other specimens. These results suggest that the newly developed composite shear walls are prone to local buckling when the spacing of the rebar trusses is relatively wide, as seen in specimens SCW-3 and SCW-4, with spacings of 140 mm and 200 mm, respectively.

The local buckling of specimen SCW-1 continued to develop with the progression of loading, and at the first cycle of a peak drift angle of 1/100, the steel faceplates continued to bulge 10-15 mm. However, the steel faceplates of specimens SCW-3 and SCW-4 developed high-mode local buckling, slight 2-5 mm local buckling was observed on the left side of the front steel faceplates approximately 50 mm away from the wall ends, and 5-7 mm local buckling was also observed at the height of 200 mm from the faceplates of specimen SCW-4, which easily provides high plate compression strength.

Steel faceplates of specimens SCW-2, SCW-5 and SCW-6 did not develop local buckling until the end of loading cycles with the peak value of 1/100. About 2-3 mm bulge can be observed on the right side of front faceplate, located 100

mm above the wall ends, as shown in Fig.7(a).

At the same loading step, some new local buckling occurred in the specimen SCW-3. A 15 mm bulge was observed on the front steel faceplate at the height of 250 mm, and a 3-5 mm bulge appeared on the right side of the steel faceplate at the height of 50 mm. Additionally, the outer side steel plate of CFST began to develop slight local buckling with about 3-5 mm bulge. For specimen SCW-4, "bang bang" sound was heard around the welding point between the rebar trusses and the steel faceplates, indicating that the welding point began to break and the constraint of the rebar trusses to the steel faceplates began to fail, the bulging increased to 10-15 mm at the height of 200 mm on the front wall.

When the peak value reached 1/66, all specimens reached the peak load at the first cycle of loading. Cracking sounds of concrete were heard through the loading step for specimen SCW-1, where local buckling continued to deteriorate at the steel faceplate and outer steel plate of CFST, the bulging was about 25-30 mm at the end of this loading step. During this loading step, specimens SCW-2, SCW-5 and SCW-6 also degraded with the further development of local buckling of steel faceplates, along with local buckling of CFST, as depicted in Fig. 7 (b), and "bang bang" sound indicated that the rebar trusses and the steel plate started to break during the process. As for specimens SCW-3 and SCW-4, high-mode buckling developed along the steel faceplate and outer steel plate of CFST, the local buckling range enlarged to about 50-300 mm, and the height of the bulges reached 30-40 mm at the end of loading step, accompanied by the crack sound of concrete and intermittent 'Bang Bang' breaking sound of the welding point.

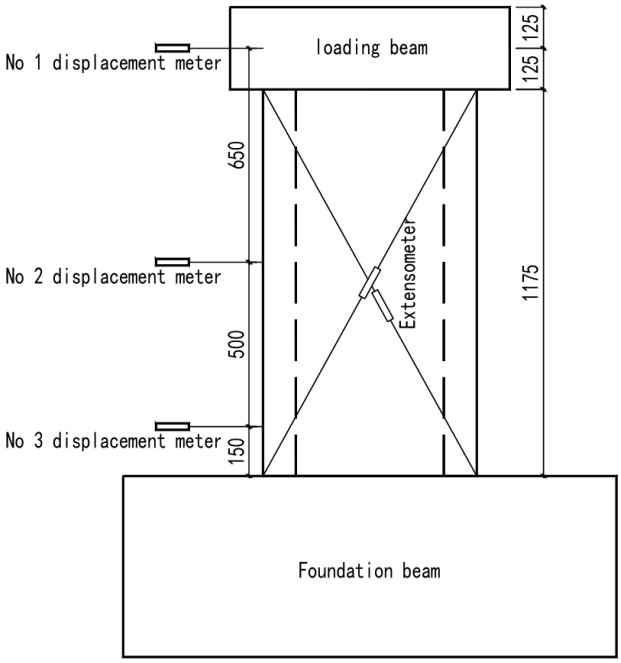

Fig. 5 Configuration of displacement meters

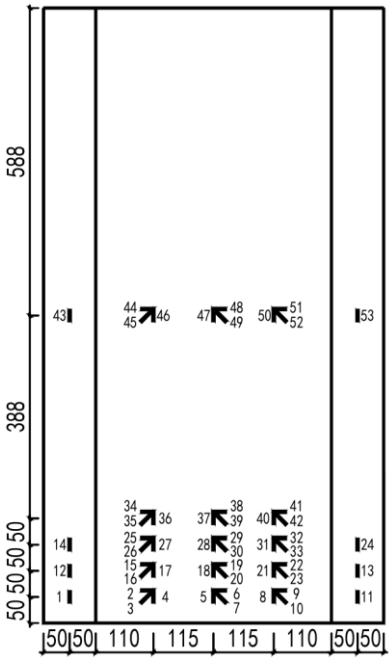

Fig. 6 Arrangement of strain gauges on steel plates

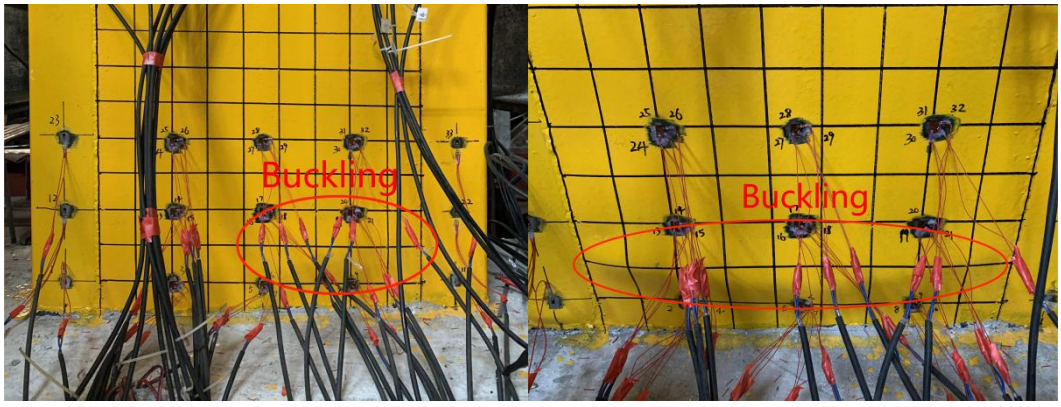

(a) Drift angle of 1/100 (b) Drift angle of 1/66

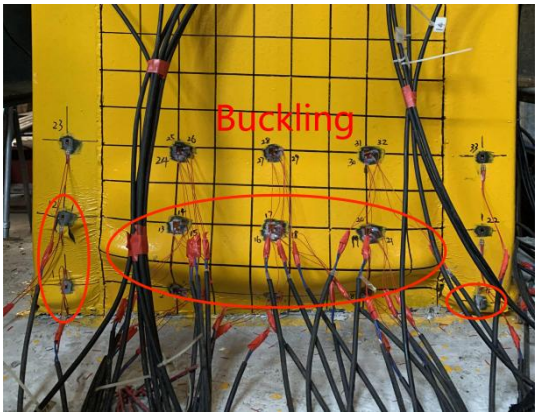

(c) Drift angle of 1/50

Fig. 7 Damage progression of the specimen SCW-2

Table 3
Drift angle of each specimen corresponding to key damage characteristics

Specimen	θ_1	θ_2	θ_3	θ_4	θ_5	θ_6
SCW-1	1/550(1)	1/300(1)	1/200(1)	——	1/55(1)	1/55(1)
SCW-2	1/300(1)	1/300(3)	1/100(3)	1/66(3)	1/30(1)	1/20(2)
SCW-3	1/300(1)	1/300(3)	1/200(3)	1/66(1)	1/50(3)	1/30(3)
SCW-4	1/300(1)	1/300(3)	1/150(1)	1/100(3)	1/30(1)	1/30(1)
SCW-5	1/300(1)	1/300(3)	1/100(3)	1/66(3)	1/50(3)	1/20(2)
SCW-6	1/300(1)	1/300(3)	1/100(3)	1/50(3)	1/50(3)	1/30(3)

Note: The number in brackets indicates loading cycle in each loading step. θ_1 is the yield displacement angle of CFST's outer steel plate, θ_2 is the displacement angle of local bond slip between steel faceplate and infill concrete, θ_3 is the displacement angle during local buckling of steel faceplate, θ_4 is the displacement angle when the welding point between rebar trusses and the steel faceplate breaks, θ_5 is the displacement angle when steel plate cracking or concrete crushing occurs in CFST, θ_6 is the displacement angle at the end of the experiment.

In cyclic loading with the peak drift angle of 1/55, specimen SCW-1 could not maintain the applied axial load due to serious buckling of the steel faceplate and outer steel plate of CFST. Additionally, with the crushing of the infill concrete, the lateral load decreased to 54% of the peak load, leading to the conclusion of the test.

At the peak drift angle of 1/50, with the further development of local buckling of the steel faceplate and outer steel plate of CFST (shown in Fig. 7(c)), the lateral loads of specimens SCW-2 to SCW-6 declined to 70%, 64%, 61%, 82% and 71% of the peak load, respectively. However, the specimens still exhibited considerable bearing capacity.

When the load was applied to the drift angle of 1/30, fracture occurred at the welding seam near the bottom of CFST after three loading cycles, the infill concrete was crushed out, and the lateral loads of specimens SCW-2 to SCW-6 degraded to 63%, 57%, 62%, 74% and 64%, respectively. Among all the specimens, specimen SCW-6 suffered the most serious damage, the welding seam between CFST and the steel faceplate of shear wall body was torn open, and the infill concrete was crushed into pieces. At the end of this loading step, the specimen could not maintain the applied axial load, and it suffered serious out-of-plane instability, therefore the test was concluded. It can be concluded that the discontinuity of the steel plate on the inner side of CFST exacerbates the degree of damage to the specimen. This is because the steel plate inside the concealed column is continuous, and the concealed column is a complete rectangular steel pipe. If the steel plate inside the concealed column is disconnected, the concealed column is a C-shaped channel steel. The bending stiffness and bearing capacity of the rectangular steel pipe are much stronger than those of the channel steel of the same section. Therefore, the stability of the wall outside the plane after the steel plate inside the concealed column is disconnected is weaker than that of the wall with continuous steel plate inside the concealed column.

Specimens SCW-2 and SCW-5 experienced similar damage when loaded to drift angel of 1/20. The lateral load decreased to 25% and 23% of the peak load, respectively. As a result, the specimens were unable to maintain the applied axial load, leading to the termination of the tests.

Fig. 7 illustrates the main damage progression of specimen SCW-2, Fig. 8 depicts the final failure state of each specimen, Fig. 9 shows the failure condition of the infill concrete after the steel faceplate was removed, and Table 3 summarizes the drift angles of each specimen corresponding to key damage characteristics.

The damage progression of the specimens demonstrates that the newly developed composite shear wall achieved the desired flexural failure mode. The failure process followed a consistent sequence: (1)Yielding of the outer steel plate of the CFST; (2) Bonding failure at the interface between the steel faceplate and the infill concrete; (3) Local buckling in the bottom part of the wall, approximately 250 mm above the foundation beam; (4) Disconnection of welding points between the rebar trusses and the steel faceplate; (5) Crushing of the concrete and fracture of the CFST's steel plate.

The following conclusions can be drawn by comparing the damage progression and failure modes of each specimen with those of SCW-2:

(1) From specimens SCW-1 and SCW-2, it is evident that rebar trusses effectively restrain local buckling of the steel faceplate, reducing the extent of buckling under the same loading drift angle.

(2) Specimens SCW-2, SCW-3, and SCW-4 had rebar truss spacings of 100 mm, 140 mm, and 200 mm, respectively. It was observed that denser truss spacing delayed the onset of buckling and reduced the severity of buckling in the steel faceplate under the same drift angle. Therefore, closer spacing of rebar trusses is strongly recommended to enhance the performance of the shear wall.

(3) The rebar trusses in specimens SCW-2 and SCW-5 were arranged horizontally and vertically, respectively. Both specimens exhibited similar damage progression and failure modes; however, SCW-5 experienced less severe damage. This improvement can be attributed to the vertical rebar trusses, which enhanced the global stability of the shear wall.

(4) Specimen SCW-2 featured a continuous CFST inner steel plate, whereas SCW-6 had a discontinuous configuration. Both specimens performed similarly up to a drift angle of 1/50. However, SCW-6 experienced earlier failure due to inadequate out-of-plane restraint on the steel faceplate caused by the discontinuity of the CFST's inner steel plate. Therefore, for ease of construction, this structural form is not recommended due to its adverse impact on wall performance.

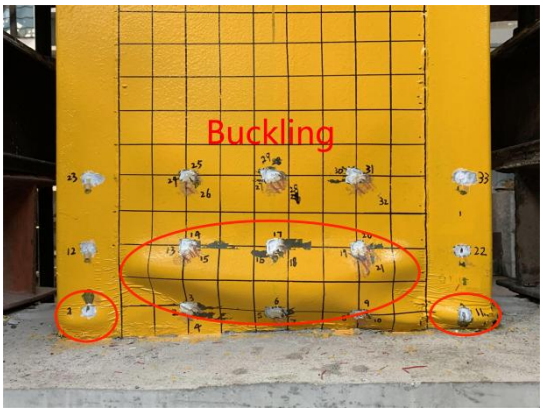

(a) Failure mode of steel plate in SCW-1

(b) Failure mode of steel plate in SCW-2

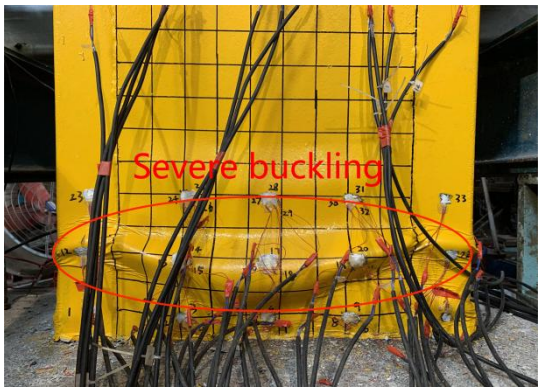

(c) Failure mode of steel plate in SCW-3

(d) Failure mode of steel plate in SCW-4

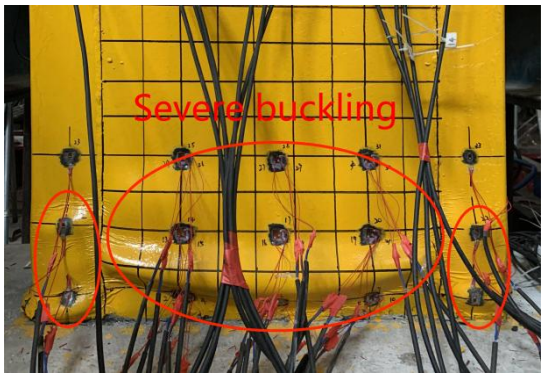

(e) Failure mode of steel plate in SCW-5

(f) Failure mode of steel plate in SCW-6

Fig. 8 Failure mode of steel plate in specimens

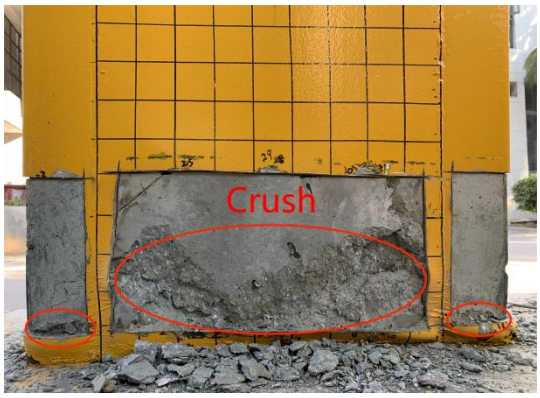

(a) Failure mode of internal concrete in SCW-1

(b) Failure mode of internal concrete in SCW-2

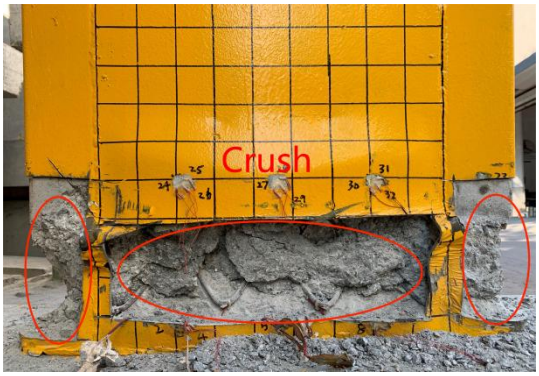

(c) Failure mode of internal concrete in SCW-3

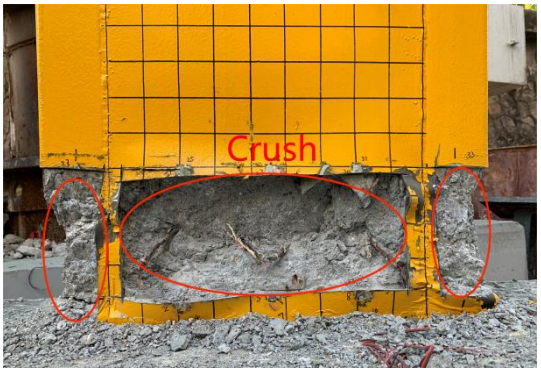

(d) Failure mode of internal concrete in SCW-4

(e) Failure mode of internal concrete in SCW-5

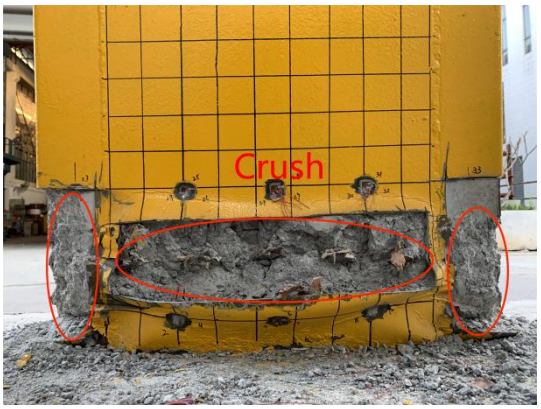

(f) Failure mode of internal concrete in SCW-6

Fig. 9 Failure mode of internal concrete in specimens

3.2. Hysteresis and skeleton curves

Figs. 10 and 11 illustrate the hysteretic and backbone curves of each specimen, derived from the lateral load and lateral displacement data. It is evident that, with the exception of specimen SCW-1, all the newly developed DSCWs exhibited significantly more stable hysteretic behavior up to a drift angle of 1/50. The initial lateral stiffness of the specimens with rebar trusses was found to be nearly identical, indicating that the spacing and orientation of the rebar trusses have minimal influence on the initial lateral stiffness.

The proposed shear walls reached their peak load at a drift angle of 1/66. Although the lateral bearing capacity dropped below 85% of the peak load at a drift angle of 1/50, the shear walls still demonstrated favorable hysteretic behavior. However, during subsequent loading phases, the strength and stiffness of the specimens deteriorated significantly due to progressive local damage. A comparative analysis of the specimens provides valuable insights into their performance:

(1) The new shear wall with closer spacing of rebar trusses exhibited a much more stable hysteretic response, deformation capacity, and energy dissipation capacity, as shown in Fig. 10(b) and Fig. 11(b). When comparing specimens SCW-2, SCW-3, and SCW-4, the peak loads were 622.2 kN, 582.5 kN, and 576.2 kN, respectively, as listed in Table 4. The bearing capacity of SCW-2 was 7% higher than SCW-3 and SCW-4, but the peak loads for SCW-3 and SCW-4, with rebar truss spacings of 140 mm and 200 mm, respectively, were essentially the same. These results suggest that rebar truss spacing has a notable effect on the specimen's strength when the spacing is less than 140 mm. Moreover, closer rebar truss spacing is a critical parameter influencing the post-peak strength, stiffness, and ductility, which deteriorated more slowly with tighter spacing.

(2) A comparison of SCW-2 and SCW-5, which featured horizontal and vertical rebar trusses respectively, revealed similar behavior throughout the entire loading process. The peak loads of these specimens were 622.2 kN and 614.8 kN, respectively. However, the vertical rebar trusses in SCW-5 contributed to maintaining more stable strength and stiffness after the peak load, as clearly illustrated in Fig. 11(c).

(3) Despite the discontinuity of the CFST's inner steel plate, specimen SCW-6 exhibited nearly the same initial stiffness, peak load, and strength and stiffness degradation up to a drift angle of 1/30. However, the discontinuity of the CFST's inner steel plate compromised the ductility of the shear wall, reducing its ability to sustain deformation under large loading cycles.

(4) Specimen SCW-1, which lacked rebar trusses, exhibited significantly worse hysteretic responses, with notably reduced hysteretic loops. In contrast, the peak loads of the new shear walls were 132%, 124%, 123%, 131%, and 129% of SCW-1, respectively. Furthermore, the new shear walls demonstrated much more stable deformation capacity and energy dissipation capacity after reaching their peak load, highlighting the improvements achieved with the new design.

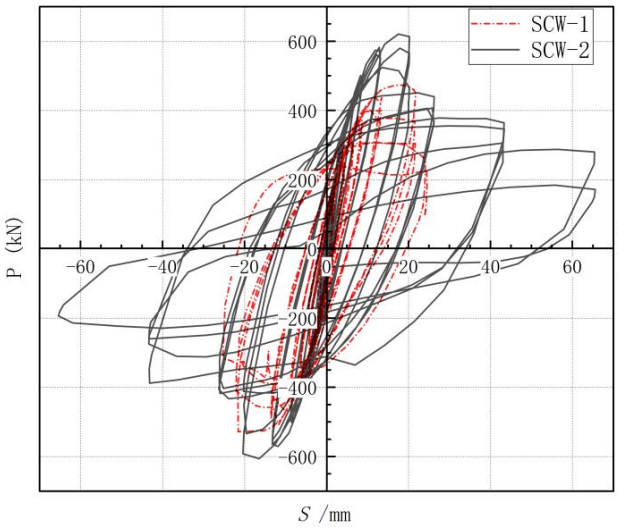

(a) With or without rebar trusses

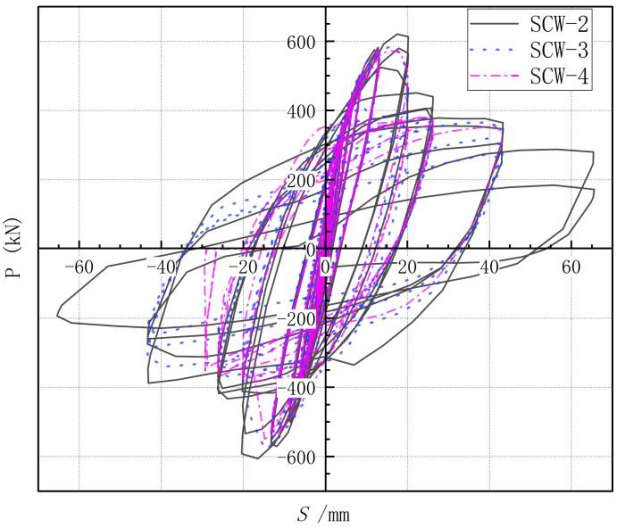

(b) Rebar truss spacing

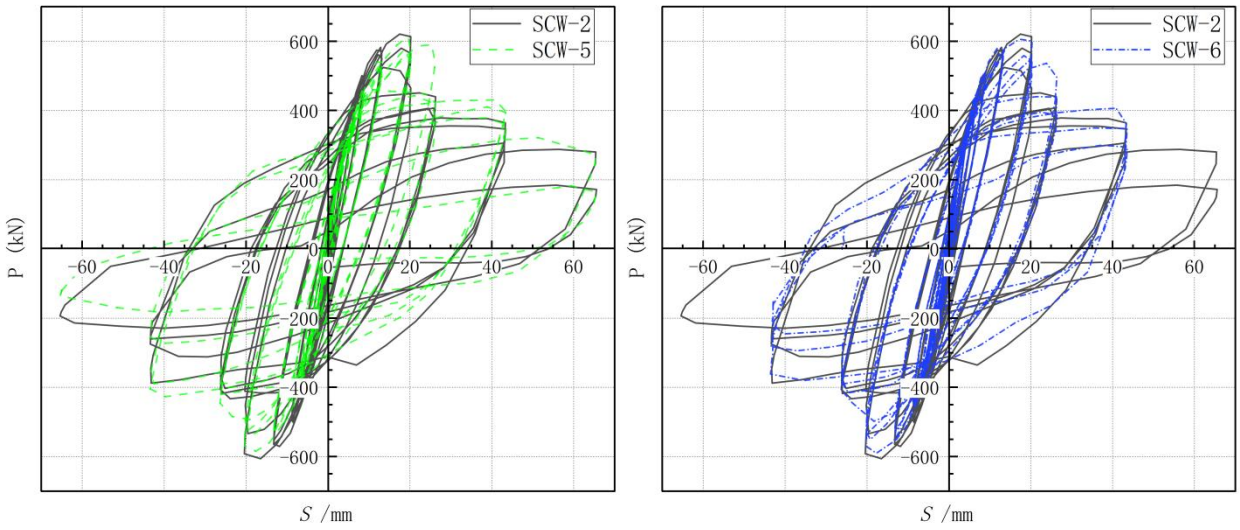

(c) Horizontal and vertical rebar trusses (d) Discontinuity of CFST' inner steel plate

Fig. 10 Comparison of hysteretic behavior of specimens

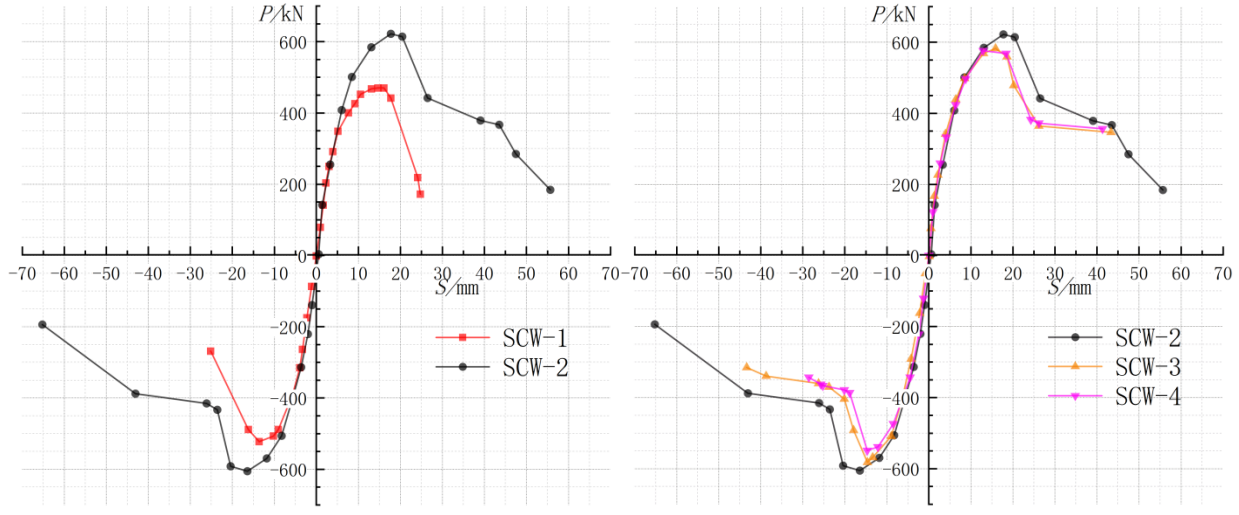

(a) With or without rebar trusses (b) Rebar truss spacing

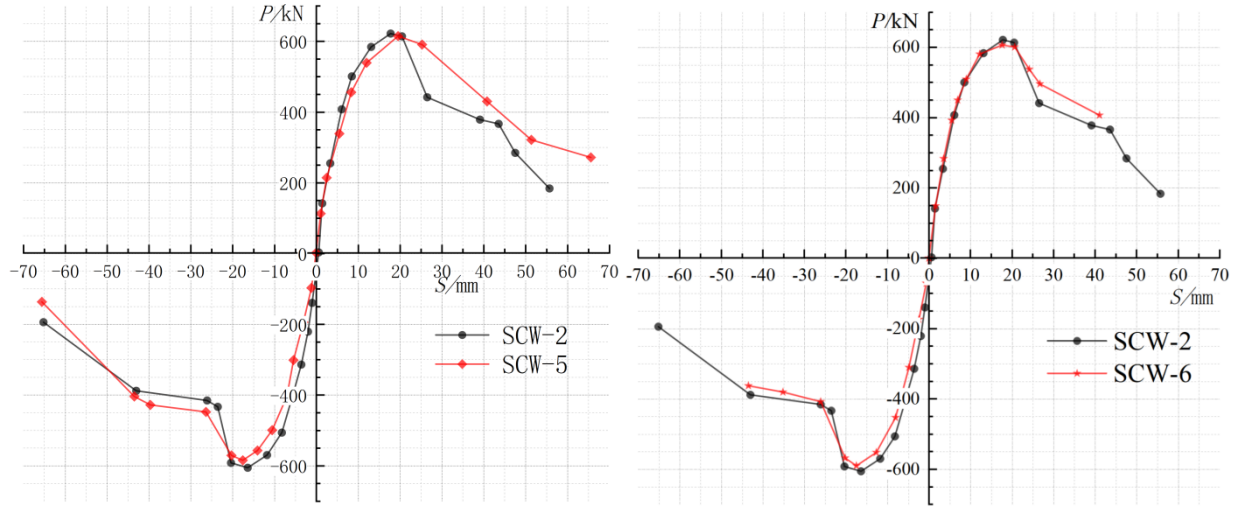

(c) Horizontal and vertical rebar trusses (d) Discontinuity of CFST' inner steel plate

Fig. 11 Skeleton curves of horizontal load-displacement at the top of specimen

3.3. Characteristic values of the specimens

To further analyze the effects of various parameters on the seismic performance of the new composite shear wall, the yield load and yield displacement are defined as the load and drift angle corresponding to the intersection of the secant stiffness at 75% of the specimen's peak bearing capacity and the elastic-plastic line, as illustrated in Fig. 12. Similarly, the failure load and failure displacement are determined as the load and drift angle corresponding to the point on the descending section of the skeleton curve where the load drops to 85% of the peak load [35], as summarized in Table 4.

Key characteristic values, including critical loads, corresponding drift angles, and ductility coefficients for each specimen, are provided in Table 4. The displacement ductility coefficient is calculated as the ratio of the failure displacement to the yield displacement. This coefficient ranges from 1.86 to 2.78,

with an average value of 2.30, indicating that DSCWs with rebar trusses exhibit good deformation capacity under an axial compression ratio of 0.40. This suggests their suitability for widespread application in real engineering projects.

The limit drift angle ranges from 1/77 to 1/41, with an average value of 1/59, exceeding the specified limit of 1/120 for shear wall structures as stipulated in the Chinese seismic code [36].

A comparison of the yield point, peak load, and failure load demonstrates that rebar trusses significantly enhance the lateral bearing capacity of the shear walls. However, variations in the spacing and orientation of the rebar trusses have minimal influence on the key load values, with the maximum observed difference being less than 7.4%.

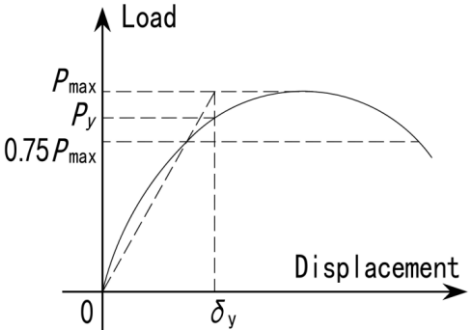

Fig. 12 Definition of yield displacement

Table 4
Key loads, drift angles and ductility coefficients of specimens

Specimen number	Loading direction	Yield point		Peak load point		Failure point		Displacement ductility coefficient
		$F_{y,EXP}$/kN	$\theta_{y,EXP}$	$F_{p,EXP}$/kN	$\theta_{p,EXP}$	$F_{u,EXP}$/kN	$\theta_{u,EXP}$	
SCW-1	positive	390.3	1/182	470.4	1/81	399.8	1/69	2.64
	negative	447.2	1/170	522.3	1/96	444.0	1/72	2.36
SCW-2	positive	530.4	1/129	622.2	1/73	528.9	1/56	2.30
	negative	524.4	1/140	605.1	1/79	514.3	1/59	2.37
SCW-3	positive	496.7	1/153	582.5	1/82	495.1	1/65	2.35
	negative	517.0	1/136	581.8	1/89	494.5	1/73	1.86
SCW-4	positive	498.9	1/146	576.2	1/101	489.8	1/62	2.35
	negative	478.6	1/148	548.5	1/89	466.2	1/77	1.92
SCW-5	positive	525.7	1/114	614.8	1/67	522.6	1/41	2.78
	negative	507.7	1/117	584.2	1/74	496.6	1/54	2.17
SCW-6	positive	519.7	1/139	607.4	1/74	516.3	1/51	2.73
	negative	503.4	1/124	589.2	1/74	500.8	1/57	2.18

Note: $F_{y,EXP}$ indicates yield load, $\theta_{y,EXP}$ is the yield drift angle, $F_{p,EXP}$ is the peak load, $\theta_{p,EXP}$ is the peak drift angle, $F_{u,EXP}$ is the failure load, $\theta_{u,EXP}$ is the failure drift angle.

Another important parameter for assessing the seismic performance of shear walls is loop stiffness [37], which reflects the stiffness degradation of the specimen. Fig. 13 illustrates the loop stiffness-lateral displacement curves of the specimens under various configurations. As shown, the loop stiffness of specimens with rebar trusses is 8.7%–34.7% higher than that of specimens without rebar trusses. Reducing the spacing of rebar trusses marginally enhances the loop stiffness and delays stiffness degradation. The loop stiffness curves of specimens SCW-2 and SCW-5 are almost identical, indicating that the orientation of the rebar trusses has minimal impact on stiffness degradation. For specimen SCW-6, which has a discontinuous steel plate inside the CFST, the loop stiffness is slightly lower than that of SCW-2 with a continuous steel plate. Additionally, the stiffness degradation of SCW-6 becomes more significant in the later stages of loading.

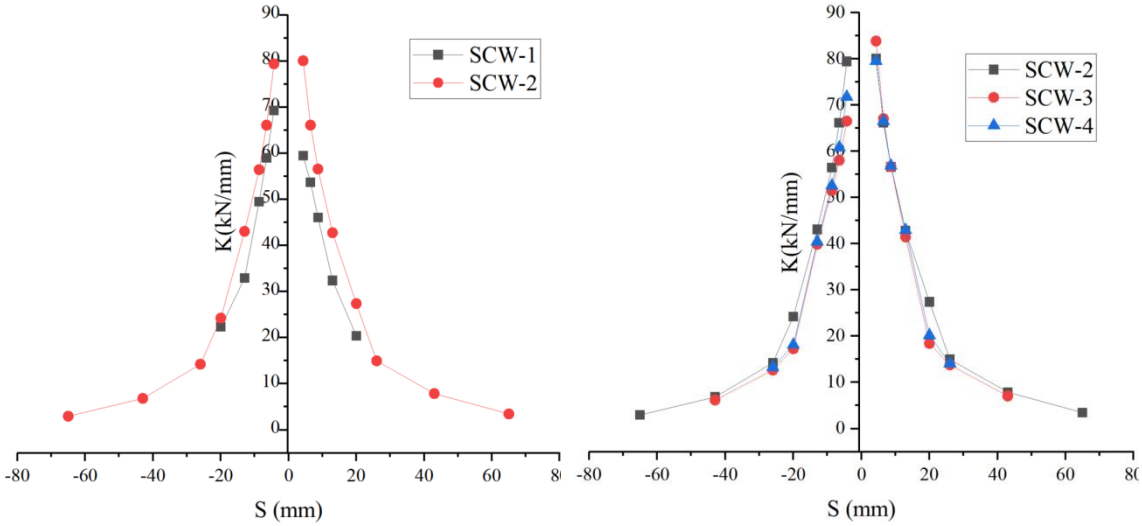

(a) With and without rebar trusses

(b) Different rebar trusses spacing

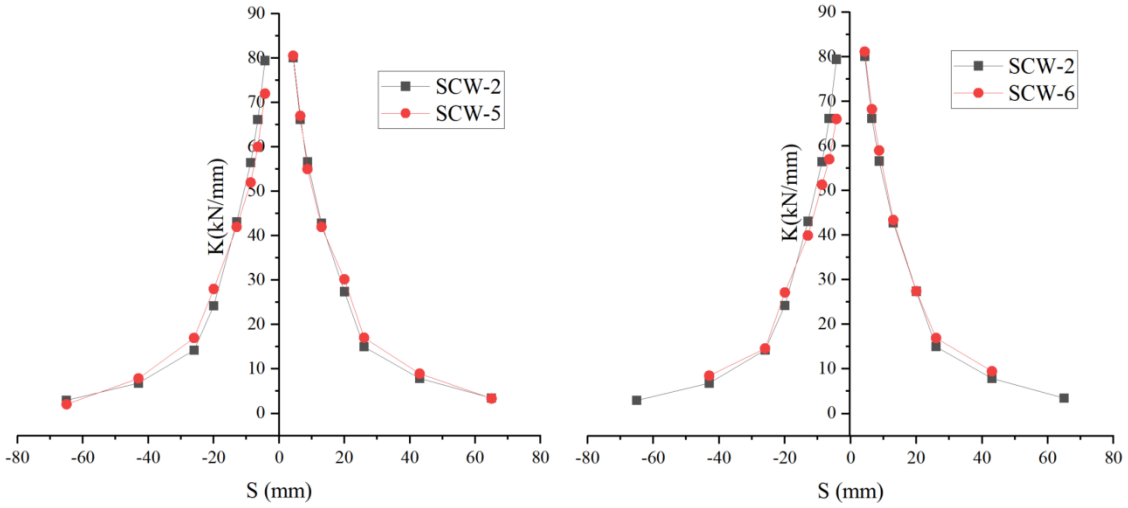

(c) Different arrangement direction of rebar trusses (d) Continuous and disconnected steel plate inside CFST

Fig. 13 Comparison of stiffness degradation curves of specimens under different parameters

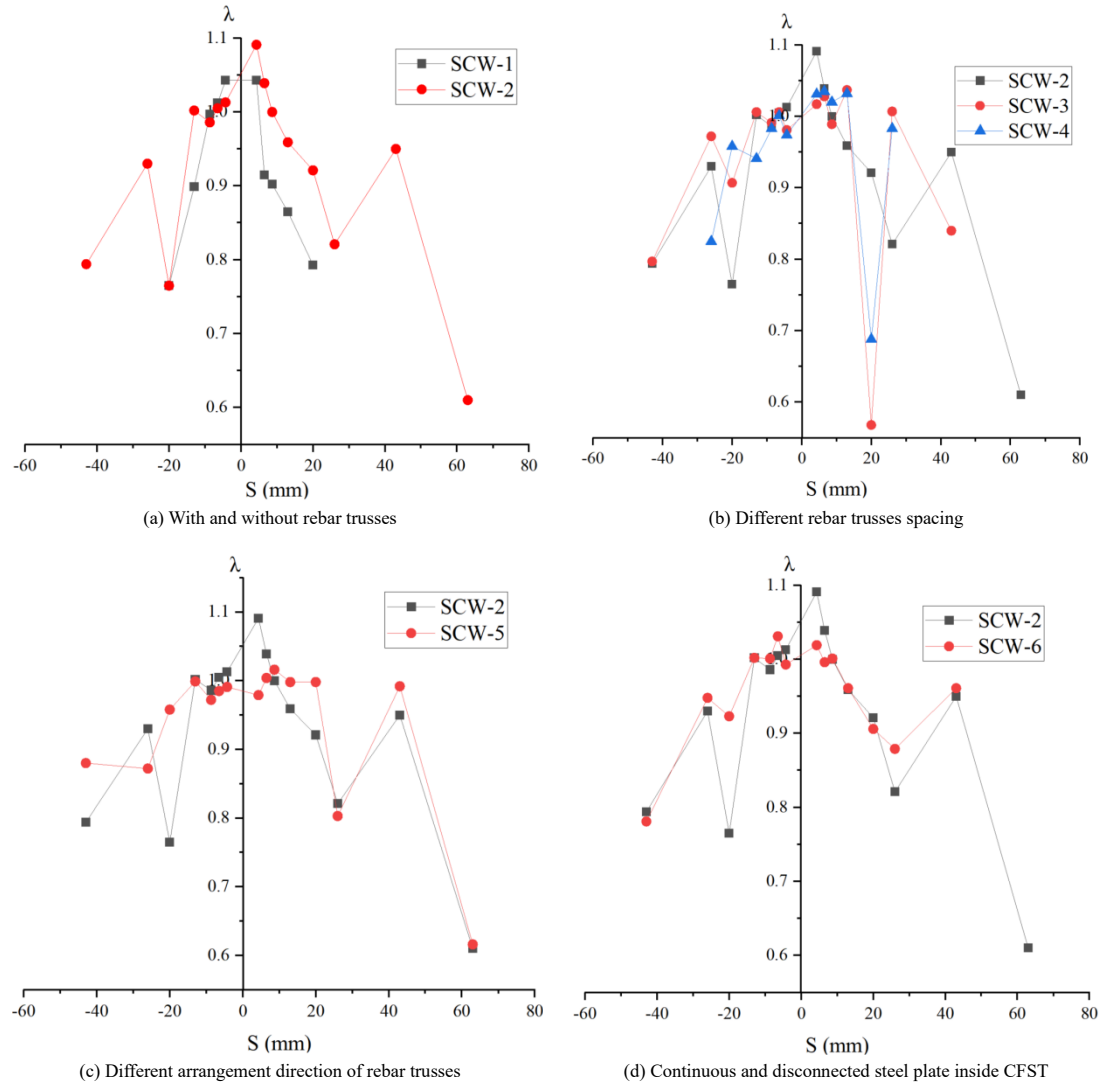

(a) With and without rebar trusses (b) Different rebar trusses spacing

(c) Different arrangement direction of rebar trusses (d) Continuous and disconnected steel plate inside CFST

Fig. 14 Second cycle strength degradation curves of each specimen under different parameters

Strength degradation is another critical parameter for evaluating shear wall performance. The strength degradation coefficient (λi) is used to quantify the ratio of the peak load of the i-th cycle to that of the first cycle at a given loading amplitude [37]. Fig. 14 shows the second-cycle strength degradation curves of the specimens under various configurations. As illustrated, the strength degradation coefficient decreases as the loading drift angle increases. The arrangement and denser spacing of rebar trusses significantly help the shear wall maintain stable strength, especially during the later loading stages when major damage occurs. Although specimens SCW-2 and SCW-5 exhibit a similar strength degradation process, the shear wall with vertical rebar trusses (SCW-5) demonstrates more stable strength retention. Additionally, the discontinuity of the CFST's inner steel plate in specimen SCW-6 does not compromise its overall strength capacity. Fig. 14(d) shows that SCW-6 maintains stable strength capacity even during the very late stages of loading when major damage occurs.

To further evaluate the energy dissipation capacity, energy consumption-half cycle curves, cumulative energy consumption-half cycle curves and equivalent viscous damping coefficient versus number of cycles were analyzed, as show in Fig. 15 to Fig. 17. In general, the energy consumption of the

specimens increases continuously with the number of loading cycles. Compared with SCW-1, the energy dissipation capacity of DSCWs is significantly enhanced by the inclusion of rebar trusses. The cumulative energy consumption of specimens with rebar trusses is 4.38–8.68 times that of specimen SCW-1.

When comparing specimens SCW-2, SCW-3, and SCW-4, reducing the spacing of rebar trusses significantly improves energy dissipation capacity. The cumulative energy consumption of SCW-2 is 1.37 times and 1.84 times that of SCW-3 and SCW-4, respectively. Comparing SCW-2 and SCW-6, the energy consumption of specimens with continuous and discontinuous steel plates inside the concealed column is similar under the same half-cycle number. However, due to its stronger stiffness at later stages, the cumulative energy consumption of SCW-2 is higher than that of SCW-6.

When comparing SCW-2 and SCW-5, both specimens exhibit nearly identical energy dissipation capacity. However, during the later loading stages, the shear wall with vertical rebar trusses (SCW-5) demonstrates better deformation capability, enabling it to consume more energy.

Fig. 17 shows the equivalent viscous damping coefficient energy dissipation cycle curve, where the equivalent viscous damping coefficients are all greater than the 0.05 value specified in the Chinese seismic code. The equivalent viscous damping coefficient shows a curve of first decreasing and then increasing with the number of energy dissipation cycles, and the turning point occurs at the 5th cycle, which is 1/300 displacement angle. This is a direct reflection of the evolution of internal material damage and the periodic activation of energy dissipation mechanism. When the displacement angle is less than 1/300, concrete cracking and interface slip cause stiffness collapse degradation, and energy dissipation growth lags behind. When the displacement angle is greater than 1/300, an efficient synergistic energy dissipation mechanism is formed by steel plate yielding, concrete crack friction, steel reinforcement plasticity, and interface slip.

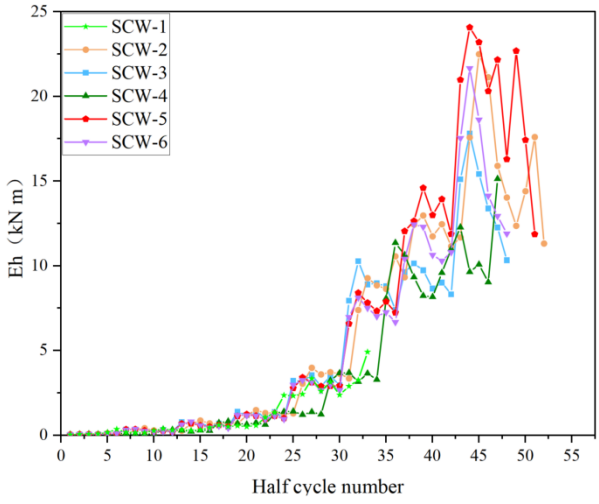

Fig. 15 Energy consumption-half cycle curves

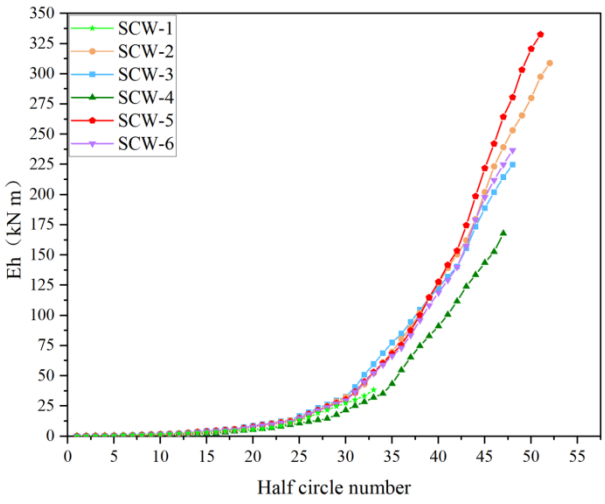

Fig. 16 Cumulative energy consumption-half cycle curves

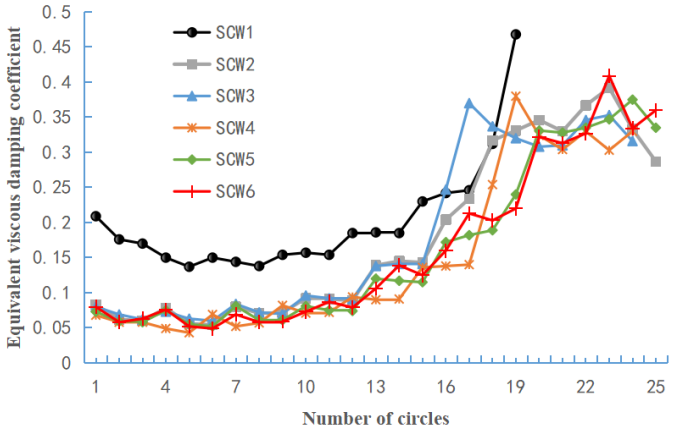

Fig. 17 Equivalent viscous damping coefficient versus number of cycles

4. Compressive and bending bearing capacity of DSCW

To evaluate the compressive and bending bearing capacities of the newly developed DSCW, the European Code Eurocode 4 [38] and the Chinese Code CECS: 546-2018 [39] were used for calculation and comparison.

4.1. European code - Eurocode 4 (2004)

Eurocode 4 adopts the full-section plastic method for calculating the compressive and bending bearing capacities of composite components. This method considers the influence of shear force while ignoring the tensile strength of concrete. The calculation formulas are as follows:

$$M_{Ed} = \alpha_M M_{Pl,N,Rd} \tag{2}$$

$$M_{pl,N,Rd} = f_{cd} A_c d_c + f_y A_{sc} d_{sc} + (1-\rho) f_y A_{swc} d_{swc} + f_y A_{st} d_{st} + (1-\rho) f_y A_{swt} d_{swt} \tag{3}$$

$$N_{Ed} = f_{cd} A_c + f_y A_{sc} + (1-\rho) f_y A_{swc} - f_y A_{st} - (1-\rho) f_y A_{swt} \tag{4}$$

$$\rho = \left(2V_{Ed} / V_{Rd} - 1\right)^2 \tag{5}$$

In the formula, M_{Ed} is the flexural bearing capacity of the composite shear wall, $M_{Pl,N,Rd}$ is the flexural bearing capacities of the composite shear wall without considering reduction, α_M is the steel grade adjustment factor, f_{cd} is the compressive strength of the concrete cylinder, A_c is the area of the concrete in the compression zone, d_c is the distance from the compressive concrete to the center of the composite wall, f_y is the yield strength of steel plate, A_{sc} and A_{st} are the areas of the compressive and tensile flange steel plates from the center of the composite wall, d_{sc} and d_{st} are the distances of the compressive and tensile flange

steel plates from the center of the composite wall, A_{swc} and A_{swt} are the areas of the compressive and tensile steel web plates, d_{swc} and d_{swt} are the distances of the compressive and tensile steel web plates from the center of the composite wall, and ρ is the reduction factor of steel plate strength considering the affection of shear force, where V_{Ed} is the design shear force and V_{Rd} is the shear bearing capacity.

4.2. Chinese code - CECS: 546 (2018)

The "Technical Standard for Steel Tube Concrete Bundle Composite Structures" (CECS: 546-2018) is based on the ultimate state theory and provides simplified N-M relationship formulas for composite shear walls under combined compression and bending. For practical design purposes, the following formulas are used:

$$\frac{N}{N_{\mathrm{u}}}+\left(1-\alpha_{\mathrm{c}}\right)\frac{M_x}{M_{ux}}\le 1 \tag{6}$$

$$\alpha_c = f_c A_{c0} / N_u \tag{7}$$

$$N_u = f_y A_{s0} + f_c A_{c0} \tag{8}$$

$$M_{ux} = \left[0.5A_{s0}\left(h-2t_s-d_{nx}\right)+bt_s\left(t_s+d_{nx}\right)\right]f_y \tag{9}$$

$$d_{nx} = \left(A_{s0}-2bt_s\right)/\left[\left(b-2t_s\right)f_c/f_y+4t_s\right] \tag{10}$$

In the formula, N is the axial compressive force of the composite wall, N_u is the axial compressive bearing capacity of the composite wall, α_c is the concrete working bearing coefficient, M_x is the bending bearing capacity of the composite wall, M_{ux} is the bending bearing capacity of the composite wall when only bending moment is applied, f_c is the compressive strength of the concrete, A_{c0} is the cross-sectional area of the concrete, f_y is the yield strength of the steel plate, A_{s0} is the cross-sectional area of the steel plate, t_s is the thickness of the steel plate, b and h are the thickness and width of the composite wall, and d_{nx} is the height of the concrete compression zone.

4.3. Comparison between Eurocde 4 and CECS:546

Using the two theoretical models provided by Eurocode 4 and CECS: 546, the compressive and bending bearing capacities of specimens SCW-2 to SCW-6 were calculated, and the results are presented in Table 5.

From Table 5, it can be observed that the calculated values for all five specimens with rebar trusses are lower than the experimental results. Specifically, the European standard (Eurocode 4) underestimates the experimental values by approximately 20%; while the Chinese standard (CECS: 546-2018) provides more accurate results, with deviations averaging only 8%.

These findings indicate that, for the DSCWs with rebar trusses proposed in this study, under a given axial pressure, the theoretical model from the Chinese standard CECS: 546-2018 is more accurate for calculating the bending bearing capacity.

Table 5
Comparison of theoretical values from two standards with experimental results

Number	Test Value / kN	Eurocode 4 / kN	Ratio	CECS: 546-2018 / kN	Ratio
SWC-2	527.4	422.1	1.25	471.6	1.12
SWC-3	506.9		1.20		1.07
SWC-4	488.8		1.16		1.04
SWC-5	516.7		1.22		1.10
SWC-6	511.6		1.21		1.08

5. Conclusions

This study investigated the seismic performance of a novel double-skin composite wall (DSCW) system reinforced with rebar trusses. A series of experimental tests and analytical comparisons were conducted based on an axial compression ratio of 0.4 and a shear span ratio of 2.0 to evaluate the mechanical behavior of the proposed DSCW under low-cycle lateral loading. The following conclusions can be drawn based on the findings:

(1) The inclusion of rebar trusses significantly improves the seismic performance of DSCWs compared to conventional designs. The rebar trusses effectively constrain the steel faceplates, delaying local buckling and enhancing overall stability. As a result, the bearing capacity of the DSCWs was increased by approximately 7%–36%, and the energy dissipation capacity was improved by 3 to 7 times compared to specimens without rebar trusses.

(2) All tested specimens exhibited a flexure-dominated failure mode. The progression of damage followed a consistent sequence: (1) bonding failure between the steel faceplates and the concrete core, (2) local buckling of the steel faceplates, (3) disconnection of the welding points between the rebar trusses and steel faceplates, (4) local buckling of the outer steel plate of the CFST boundary columns, and (5) crushing of the infill concrete and fracture of the CFST steel plate.

(3) The mechanical properties of DSCWs are only marginally influenced by the orientation of the rebar trusses (horizontal or vertical). However, walls with vertical rebar trusses demonstrated approximately 9.1% higher flexural bearing capacity at later loading stages due to enhanced global stability provided by the vertical truss configuration.

(4) Reducing the spacing of rebar trusses effectively delays stiffness and strength degradation, improving the ductility and energy dissipation capacity of the wall. Specimens with closer truss spacing (e.g., 100 mm) exhibited more stable hysteretic behavior and slower post-peak deterioration compared to specimens with larger spacings.

(5) While introducing a discontinuous inner steel plate in the CFST boundary column can facilitate construction, it compromises the deformation capacity and out-of-plane stability of the wall after reaching peak load. This structural form is therefore not recommended for practical applications where high deformation capacity is required.

(6) The displacement ductility coefficients of the specimens ranged from 1.86 to 2.78, with an average value of 2.30, indicating excellent deformation capacity. The ultimate drift angles varied from 1/77 to 1/41, with an average of 1/59, exceeding the seismic design limit of 1/120 specified in the Code for Seismic Design of Buildings. This demonstrates that the proposed DSCWs can sustain substantial deformations before failure, making them suitable for seismic applications.

(7) The theoretical model provided by the Chinese Code CECS: 546-2018 more accurately predicts the bending bearing capacities of the DSCWs, with deviations averaging only 8% compared to experimental results. In contrast, the European Code Eurocode 4 underestimates the bearing capacities by about 20%, highlighting the suitability of the Chinese code for designing DSCWs with rebar trusses.

(8) Considering the small number of specimens in this article, further in-depth research will be conducted on the seismic performance of this component under the variation parameters of axial compression ratio and shear span ratio, combining experiments and finite element analysis.

Declaration of competing interest

Financial and personal entanglements, either with entities or individuals bearing potential sway over our scholarly endeavors, are categorically nonexistent, it is declablue. Absent from the ambit of our professional lives are interests—both tangible and intangible—that might be perceived as exerting influence upon the stance articulated within, or critiqued in, a discourse designated: "Experimental Investigation into the Seismic Response of Double-Skin Composite Walls Reinforced by Rebar Trusses," demonstrably shown thus.

Acknowledgements

This work was supported by the National Natural Science Foundation of China (Grant No.52178139) and the Natural Science Foundation of Guangdong Province (Grant No. 2021B1111610009).

References

[1] Wu Gang, Feng Decheng, Xu Zhao, et al. Research developments in precast concrete structural systems [J]. Journal of Civil Engineering and Management, 38 (2021) 41−51.(in Chinese).
[2] Salmon D C, Tadros M K, Culp T. A New Structurally and Thermally Efficient Precast Sandwich Panel System [J]. PCI Journal, 1994,39(4): 90-101.
[3] Chu Mingjin, Liu Jiliang, Cui Huichen, et al. Experimental study on seismic behaviors of assembled monolithic concrete shear walls built with precast two-way hollow slabs with various details[J]. Journal of Building Structures, 2014, 35(1):93-102.(in Chinese).
[4] Zhi Q, Guo Z. Experimental evaluation of precast concrete sandwich wall panels with steel–glass fiber–reinforced polymer shear connectors[J].Advances in Structural Engineering, 2017, 20(10):136943321668319.
[5] Yang Lianping, Yu Shaole, Zhang Qilin, et al. Research status quo and key issues in superimposed shear wall structure [J]. Building Structure, 2017,47(12):78-88. (in Chinese).

[6] Liu Wei, Wang Chao. Research and development of steel plate shear wall[J]. Journal of Jilin Jianzhu University, 2017(3):26-30. (in Chinese).
[7] Adams P F , Zimmerman T , Macgregor J G . Design and Behavior of Composite Ice-Resisting Walls[J]. Aci Special Publication, 87 (1988) 23-40.
[8] Hassinen P, Kouhi J , Zimmerman T , et al. Static and cyclic load tests of a composite ice-resisting wall. 1989.
[9] Stephen M J, Zimmerman T. The Strength Of Composite Ice-Resisting Walls Subjected To Combined Loads[J]. Aztex Corp, 1990.
[10] Wright H D, Gallocher S C. The behaviour of composite walling under construction and service loading[J]. Journal of Constructional Steel Research, 35(3)(1995)257-273.
[11] Wright H . The axial load behaviour of composite walling[J]. Journal of Constructional Steel Research, 45(3) (1998) 353-375.
[12] Hossain K, Wright H D. Experimental and theoretical behaviour of composite walling under in-plane shear[J]. Journal of Constructional Steel Research, 60(1) (2004) 59-83.
[13] RA Link, A. E. Elwi. Composite Concrete-Steel Plate Walls: Analysis and Behavior. [J]. J. Struct. Eng., 121(2) (1995) 260-271.
[14] Emori K . Compressive and Shear Strength of Concrete Filled Steel Box Wall[J]. International Journal of Steel Structures, 26(2) (2002) 29-40.
[15] NIE Jianguo，BU Fanmin，FAN Jiansheng． Quasi-static test on low shear-span ratio composite shear wall with double steel plates and infill concrete under high axial compression ratio [J]. Engineering Mechanics, 2013,30 (6) : 60-66. (in Chinese).
[16] BU Fanmin, NIE Jianguo, FAN Jiansheng. Experimental study on seismic behavior of medium and high shear-span ratio composite shear wall with double steel plates and infill concrete under high axial compression ratio [J]. Journal of Building Structures, 2013,34 (4) 91-98. (in Chinese).
[17] Nie Jianguo, Bu Fanmin, Fan Jiansheng. Experimental research on seismic behavior of low shear-span ratio composite shear wall with double steel plates and infill concrete [J]. Journal of Building Structures, 2011,32 (11) 74−81. (in Chinese).
[18] Jian-Guo Nie, hong-Song Hu, Jian-Sheng Fan, Mu-Xuan Tao, Sheng-Yong Li, Fu-Jun Liu. Experimental study on seismic behavior of high-strength concrete filled double-steel-plate composite walls [J]. Journal of Constructural Steel Research. 88 (2013) 206-219.
[19] Tang Xulin, Ding Changyin, Zuo Zhiliang, et al. Experimental research on seismic behavior of composite shear wall with double steel plates and infill concrete with stiffeners [J]. Journal of Building structures, 2017,38 (5) 85−91. (in Chinese).
[20] Wu Xiaodong, Tong Lewei. Experimental study on seismic behavior of steel-concrete-steel composite shear walls with CFST boundary columns and partitioning steel plates [J]. Journal of Building structures, 2019,40 (12) 41 −50. (in Chinese).
[21] Tae-Sung Eom, Hong-Gun Park, Cheol-Ho Lee, Jin-Ho Kim, In-Hwa Chang. Behavior of Double Skin Composite Wall Subjected to In-Plane Cyclic Loading [J]. Struct. Eng. 135(10) (2009) 1239-1249.
[22] Liu Hongliang, Cai Jian, Yang Chun, et al. Experimental study on seismic behavior of composite shear wall with double steel plates and infill concrete with binding bars [J]. Journal of Building Structures, 2013,34 (6) 84 −92.(in Chinese)
[23] Cai Jian, Duan Weining, Tang Xuning, et al. Influence of axial compression ratios and shear-span ratios on seismic behavior of composite shear wall with double steel plates and infill concrete with binding bars [J]. Journal of Building Structures, 2018,39 (2) 37−43.(in Chinese).
[24] JI Xiaodong, JIANG Feiming, QIAN Jiaru, et al. Experimental study on seismic behavior of steel tube-double steel plateconcrete composite shear walls [J]. Journal of Building Structures, 2013,34 (6) 75-83.(in Chinese).
[25] Zhang X M, Qin Y, Chen Z H. Experimental seismic behavior of innovative composite shear walls [J]. Journal of Constructional Steel Research, 116 (2016) 218–232.
[26] Chen Zhihua, Jiang Yuting, Zhang Xiaomeng, et al. Research on resilience model of steel tube bundle composite shear wall [J]. Earthquake Engineering and Engineering Dynamics, 2017,37 (1) 115–122. (in Chinese)
[27] Chen Zongping, Zhou Ji, Mo Linlin, et al. Experimental study on seismic behavior of double-skin corrugated plates and concrete composite shear wall [J]. Journal of Building Structures, 2022, 43(10) 75-83.(in Chinese)
[28] Zhang Zhuangnan, Li Shanshan, Wang Chungang, et al. Seismic performance of double steel plate concrete composite
shear wall with hybrid connectors [J]. Journal of Building Structures, 2023, 44(S1) 92-100.(in Chinese)
[29] Jun Shi, Shan Gao, Lanhui Guo, et al., Compressive behaviour of double skin conposite shear walls stiffened with rebar trusseses, J. Constr. Steel Res. 2021,180(5):106581.
[30] Jianhong Han, Ganping Shu, Ying Qin, et al. Experimental seismic behavior of double skin composite wall with rebar trusses, J. Constr. Steel Res 2021,180: 106569.
[31] Wei fangfang, Zhu youhua, Yu jun. Numerical analysis of shear resistance of concrete filled double-steel-plate composite walls with shear stud connectors. [J]. Journal of Civil and Environmental Engineering, 2021,43(1):96-106.(in Chinese) .
[32] Luo yongfeng, Li jian, Guo xiaonong. Numerical Analysis of hysteretic performance of double-steel-layer-concrete composite shear wall. [J]. Journal of Hunan University, 2013,41(11)57-62.(in Chinese)
[33] Cai Jian, Xie Xiaofeng, Yang Chun, et al. An Experimental Research on the Composite Column with Core of High-Strength Concrete Filled Steel Tube under Axial Compression Loading [J]. Journal of South China University of Technology (Natural Science Edition),2002, 30(6) 81-85. (in Chinese).
[34] Alzeni Y, Bruneau M. In-plane cyclic testing of concrete-filled sandwich steel panel walls with and without boundary elements. J Struct Eng 2017,143(9):04017115.
[35] Ductility of prestressed concrete piles subjected to situlated seismic loading: Park, R and Falconer T JJ. Prestressed Concr. Inst. Vol 28 No 5 (September–October 1983) 112−144.
[36] Ministry of Housing and Urban-Rural Development of the People's Republic of China.Code for seismic design of buildings:GB 500112010 [S].Beijing:China Architecture & Building Press,2016.
[37] Tang Jiuru.Seismic performance of reinforced-concrete beam-column connections[M].Nanjing:Southeast University Press,1989: 312-316 (in Chinese).
[38] BS EN 1994-1-1: 2004, Eurocode 4: Design of Composite Steel and Concrete Structures [S]. Brussels: European committee for Standardization, 2004.
[39] CECS: 546−2018, Technical Standard for Structures with Concrete-Filled Multicellular Steel Tube Walls [S]. Beijing: China Planning Press, 2018. (in Chinese)